

## Effects of the Coulomb and the spin-orbit interaction in a deformed mean field on the pairing correlations in $N = Z$ nuclei

Eunja Ha\* and Myung-Ki Cheoun†

*Department of Physics and Origin of Matter and Evolution of Galaxy (OMEG) Institute, Soongsil University, Seoul 156-743, Korea*

H. Sagawa‡

*RIKEN, Nishina Center for Accelerator-Based Science, Wako 351-0198, Japan  
and Center for Mathematics and Physics, University of Aizu, Aizu-Wakamatsu, Fukushima 965-8560, Japan*

(Received 5 August 2018; revised manuscript received 17 April 2019; published 3 June 2019)

We perform systematic calculations regarding the effects by Coulomb and/or spin-orbit (SO) interaction on like- and unlike-pairing correlations in  $sd$ -,  $pf$ -, and  $sdgh$ -shell  $N = Z$  nuclei. The former two interactions are comprised in a deformed mean-field potential and the latter pairing correlations are treated by residual interactions in the mean field. We make use of two different pairing matrix elements (PMEs) for the residual interactions: constant and state-dependent Brueckner  $G$  matrix. The constant PME may give rise to meaningful information on the pairing correlations under the Wigner spin-isospin  $SU(4)$  symmetry in the absence of the Coulomb and the SO interaction. The state-dependent Brueckner PME takes into account the nuclear medium effect based on a realistic nucleon-nucleon interaction. In this work, through the analyses of the Coulomb and the SO interaction effects on the pairing correlations, we discuss in detail the isoscalar pair condensation and the coexistence of the isoscalar and the isovector pairs in the unlike pairing of the  $N = Z$  nuclei. Our results show that the Coulomb and the SO interaction as well as nuclear deformation affect the single-particle state evolution in a deformed mean field and, as a result, give significant impacts on the pairing correlations and the smearing of occupation probabilities near Fermi energy. In particular, the pairing gaps in the heavy nuclei are largely disturbed by the Coulomb interaction as well as the SO interaction.

DOI: [10.1103/PhysRevC.99.064304](https://doi.org/10.1103/PhysRevC.99.064304)

### I. INTRODUCTION

Recently, pairing correlations in nuclei are being revived because of lots of interesting discussions whether we may expect deuteronlike structure in some specific nuclei with  $N \simeq Z$ . Most nuclei have revealed interesting features stemming from pairing correlations of neutron-neutron ( $nn$ ) and proton-proton ( $pp$ ) pairs, which is called like pairing. Bardeen-Cooper-Schrieffer (BCS) theory is often adopted in the nuclear physics to take into account the property of the pairing correlations. This theory has been established by the like-pairing correlations in a mean field with the help of the seniority scheme.

However, in some nuclei, one expects another type of the pairing correlations from neutron-proton ( $np$ ) pairs. Specifically, for  $N \simeq Z$  nuclei, protons and neutrons occupy the same orbital and may have the maximum spatial overlap. The  $nn$  and  $pp$  pairing have an isovector (IV) spin-singlet ( $T = 1, J = 0$ ) mode, while the  $np$  pairing has an isoscalar (IS) spin-triplet mode ( $T = 0, J = 1$ ) as well as an IV spin-singlet mode ( $T = 1, J = 0$ ) [1–6].

Over the last few decades, there have been many discussions of the  $np$  pairing correlations, in particular, the IS and IV pairing interaction and their competition and/or coexistence in some specific nuclei with  $N \simeq Z$  [7–10]. Most studies focused on  $N = Z$  nuclei because the  $np$  pairing is expected to be larger than that of  $N \neq Z$  nuclei. However, as shown in a recent work [11], the nuclear structure of  $N \simeq Z$  nuclei may also be affected by the  $np$  pairing correlations. For example, the authors of Ref. [11] predicted a mixing phase of the IS and IV pairing correlations for nuclei with  $60 < N < 70$  and  $57 < Z < 64$ .

Other works for understanding the role of the  $np$  pairing correlations were aimed for interpreting Wigner energy, which is associated with a linear isospin dependence in the nuclear binding energy [12]. For example, the IS  $np$  pairing was claimed to account for the Wigner energy introduced to explain unusual even-even odd-odd nuclei mass differences by the linear isospin-dependence [13,14]. In particular, the IS contribution with  $J = \text{odd}$  components was shown to be significant in their shell-model calculations. The Wigner energy was also interpreted in terms of the isospin symmetry breaking by the cranking method in the isospin space in a similar way to the rotational symmetry breaking leading to rotational bands [15]. But the IS contribution was shown to be smaller than that of the IV component of the  $np$  pairing correlations. This approach was exploited to understand the

\*ejha@ssu.ac.kr

†Corresponding author: cheoun@ssu.ac.kr

‡sagawa@ribf.riken.jp

symmetry energy as well as the Wigner energy by the explicit consideration of the isospin-dependent potential energy term,  $\frac{\kappa}{2}\mathbf{T}^2$ , beyond mean-field theories [16,17]. In Refs. [18,19], quartet correlations beyond the standard BCS-type approach were taken into account in the study of the Wigner energy. It was pointed out that in the quartet model the IV contribution is important for elucidating the empirical Wigner energies. In these studies [13–19], simple separable type pairing interactions are adopted as a model Hamiltonian. In the present work, we adopt pairing interactions based on Brueckner  $G$  matrix, which is obtained from a realistic nucleon-nucleon (N-N) interaction taking into account nuclear medium effect.

Recently, more interesting experimental data were reported, which show the IV quenching in the  $M1$  spin transition data for  $sd$ -shell  $N = Z$  nuclei [20]. It implies that the  $T = 0$  pairing by the tensor force, which is well known in deuteron structure, may become important in finite nuclei [21,22] and lead to IS pair condensation in nuclear symmetric matter and also finite nuclei. The Gamow-Teller (GT) strength distribution data for  $^{56}\text{Ni}$  in Ref. [23] also show explicitly the importance of the  $np$  pairing. Since then there appeared many theoretical discussions about the IV quenching related to the  $np$  pairing [24–26]. Detailed reports about the present status and recent progress concerning the  $np$  pairing correlations in nuclear structure can be found at Refs. [27,28].

The importance of the  $np$  pairing was also discussed in our previous papers [29–33] by using a state-dependent two-body pairing interaction given by the Brueckner  $G$  matrix based on the CD Bonn potential [34,35]. A deformed quasiparticle random phase approximation (DQRPA) was utilized to include explicitly both the deformation and the like and unlike pairings. The deformation is indispensable to discuss the pairing correlations because the shell evolution by the deformation may compete and/or cooperate with the pairing correlations in the residual interaction.

The Coulomb and the spin-orbit (SO) force are important ingredients in the mean field. The two forces may play significant roles to determine the pairing correlations and also Fermi energies. For example, Fermi energy difference of protons and neutrons, which is easily affected by the Coulomb and/or

TABLE I. Deformation parameter  $\beta_2$  from experimental  $E2$  transition data [40], theoretical  $\beta_2$  by relativistic mean field (RMF) [41], FRDM model [42], and ours for the  $sd$ -,  $pf$ -, and  $sdg_{7/2}h_{11/2}$ -shell  $N = Z$  nuclei. The values of  $\beta_2^{\text{Ours}}$  are obtained at the minimized ground-state energy. Empirical pairing gaps estimated from a five-point mass formula [29,36] are also presented. Theoretical values from NNDC data and KTUY05 data [43] are used when experimental mass data are not available.

Nucleus	$ \beta_2^{E2} $ [40]	$\beta_2^{\text{RMF}}$ [41]	$\beta_2^{\text{FRDM}}$ [42]	$\beta_2^{\text{Ours}}$	$\Delta_p^{\text{emp}}$	$\Delta_n^{\text{emp}}$
$^{24}\text{Mg}$	0.605	0.416	0.	0.300	3.123	3.193
$^{36}\text{Ar}$	0.256	-0.207	-0.255	-0.200	2.265	2.311
$^{48}\text{Cr}$	0.337	0.225	0.226	0.200	2.128	2.138
$^{64}\text{Ge}$	–	0.217	0.207	0.100	1.807	2.141
$^{108}\text{Xe}$	–	–	0.162	0.100	1.467	1.496
$^{128}\text{Gd}$	–	0.350	0.341	0.100	1.415	1.393

the SO force, may block the  $np$  pairing correlations. The deformation also changes single-particle state (SPS) density around Fermi surface, and as a result, gives rise to change of the pairing correlations [37].

The aim of the present work is to study the effects of the Coulomb and the SO force in a mean field on the pairing correlations in a deformed BCS approach. Specifically, we focus on the unlike pairing, i.e., the  $np$  pairing correlations for  $N = Z$  nuclei, such as  $^{24}\text{Mg}$  and  $^{36}\text{Ar}$  in  $sd$  shell,  $^{48}\text{Cr}$  and  $^{64}\text{Ge}$  in  $pf$  shell, and  $^{108}\text{Xe}$  and  $^{128}\text{Gd}$  in  $sdg_{7/2}h_{11/2}$ -shell nuclei. In Table I, we summarize basic properties of those nuclei. Another point of this work is to study the Wigner spin-isospin SU(4) symmetry violation by the Coulomb and the SO interaction [38,39] in the pairing correlations of the  $N = Z$  nuclei.

## II. FORMALISM FOR DEFORMED BCS

Since the theoretical framework for a deformed BCS approach (DBCS) have already been detailed in our previous papers [29,32], we briefly recapitulate the basic formula. We start from the following nuclear Hamiltonian

$$\begin{aligned}
 H &= H_0 + H_{\text{int}}, \\
 H_0 &= \sum_{\rho\alpha\alpha'} \epsilon_{\rho\alpha\alpha'} c_{\rho\alpha\alpha'}^\dagger c_{\rho\alpha\alpha'}, \\
 H_{\text{int}} &= \sum_{\rho\alpha\rho\beta\rho\gamma\rho\delta,\alpha'\beta'\gamma'\delta'} V_{\rho\alpha\alpha'\rho\beta\beta'\rho\gamma\gamma'\rho\delta\delta'} c_{\rho\alpha\alpha'}^\dagger c_{\rho\beta\beta'}^\dagger c_{\rho\gamma\gamma'} c_{\rho\delta\delta'},
 \end{aligned} \tag{1}$$

where greek letters denote proton or neutron SPSs with a projection  $\Omega$  of a total angular momentum on a nuclear symmetry axis.  $\rho_\alpha$  ( $\rho_\alpha = \pm 1$ ) denotes a sign of the total angular momentum projection of a  $\alpha$  state. Isospins of the particles are denoted by greek letters with prime. The operator  $c_{\rho\alpha\alpha'}^\dagger$  ( $c_{\rho\alpha\alpha'}$ ) in Eq. (1) stands for a usual creation (destruction) operator of a real particle in the state of  $\alpha\rho_\alpha$ . The Hamiltonian, represented by real particles in Eq. (1), was then transformed to a quasiparticle representation by the following DBCS transformation for the  $\alpha$  state

$$\begin{pmatrix} a_1^\dagger \\ a_2^\dagger \\ a_{\bar{1}} \\ a_{\bar{2}} \end{pmatrix}_\alpha = \begin{pmatrix} u_{1p} & u_{1n} & v_{1p} & v_{1n} \\ u_{2p} & u_{2n} & v_{2p} & v_{2n} \\ -v_{1p} & -v_{1n} & u_{1p} & u_{1n} \\ -v_{2p} & -v_{2n} & u_{2p} & u_{2n} \end{pmatrix}_\alpha \begin{pmatrix} c_p^\dagger \\ c_n^\dagger \\ c_{\bar{p}} \\ c_{\bar{n}} \end{pmatrix}_\alpha, \tag{2}$$

where  $u$  and  $v$  coefficients are calculated by the following DBCS equation

$$\begin{pmatrix} \epsilon_p - \lambda_p & 0 & \Delta_{p\bar{p}} & \Delta_{p\bar{n}} \\ 0 & \epsilon_n - \lambda_n & \Delta_{n\bar{p}} & \Delta_{n\bar{n}} \\ \Delta_{p\bar{p}} & \Delta_{p\bar{n}} & -\epsilon_p + \lambda_p & 0 \\ \Delta_{n\bar{p}} & \Delta_{n\bar{n}} & 0 & -\epsilon_n + \lambda_n \end{pmatrix} \begin{pmatrix} u_{\alpha''p} \\ u_{\alpha''n} \\ v_{\alpha''p} \\ v_{\alpha''n} \end{pmatrix} = E_{\alpha\alpha''} \begin{pmatrix} u_{\alpha''p} \\ u_{\alpha''n} \\ v_{\alpha''p} \\ v_{\alpha''n} \end{pmatrix}. \quad (3)$$

Here  $E_{\alpha\alpha''}$  is an energy of a quasiparticle 1 and 2 denoted  $\alpha''$  in the  $\alpha$  state. We include  $n\bar{p}$  and  $\bar{n}p$  pairings in addition to the like-pairing ( $p\bar{p}$  and  $n\bar{n}$ ) correlations. The pairing potentials in Eq. (3) are permitted between the nucleons in a time-reversed state ( $\alpha-\bar{\alpha}$ ) [4]. But the unlike pairing may have ( $\alpha-\alpha$ ) pairing as well as ( $\bar{\alpha}-\bar{\alpha}$ ) pairing [5]. An effective approach to take into account these unlike pairings is shown in Appendix A.

In the DBCS, the quasiparticle state is mixed with different particle states in a spherical basis because each deformed state (basis) is represented by a linear combination of the spherical state (basis) (see Fig. 1 at Ref. [29]). This feature is one of additional merits due to the inclusion of deformation in the DBCS approach. With the  $np$  pairing in the deformed basis one may get a simple HFB-type transformation in the spherical basis [3,29].

The pairing potentials in Eq.(3) are calculated in the deformed basis by using  $G$  matrix calculated from the realistic Bonn CD potential for the N-N interaction as follows:

$$\Delta_{p\bar{p}\alpha} = \Delta_{\alpha p\bar{p}} = - \sum_{\gamma} \left[ \sum_{J,a,c} g_{pp} F_{\alpha\alpha\bar{a}\bar{a}}^{J0} F_{\gamma c\bar{\gamma}c}^{J0} G(aacc, J, T = 1) \right] (u_{1p\gamma}^* v_{1p\gamma} + u_{2p\gamma}^* v_{2p\gamma}), \quad (4)$$

$$\begin{aligned} \Delta_{p\bar{n}\alpha} = \Delta_{\alpha p\bar{n}} = & - \sum_{\gamma} \left[ \sum_{J,a,c} g_{np}^{T=1} F_{\alpha\alpha\bar{a}\bar{a}}^{J0} F_{\gamma c\bar{\gamma}c}^{J0} G(aacc, J, T = 1) \right] \text{Re}(u_{1n\gamma}^* v_{1p\gamma} + u_{2n\gamma}^* v_{2p\gamma}) \\ & + \left[ \sum_{J,a,c} g_{np}^{T=0} F_{\alpha\alpha\bar{a}\bar{a}}^{J0} F_{\gamma c\bar{\gamma}c}^{J0} iG(aacc, J, T = 0) \right] \text{Im}(u_{1n\gamma}^* v_{1p\gamma} + u_{2n\gamma}^* v_{2p\gamma}), \end{aligned} \quad (5)$$

where  $F_{\alpha\alpha\bar{a}\bar{a}}^{JK} = B_a^\alpha B_a^\alpha (-1)^{j_a - \Omega_\alpha} C_{j_a \Omega_\alpha, j_{\bar{a}} - \Omega_\alpha}^{JK} (K = \Omega_\alpha - \Omega_{\bar{a}})$  was introduced with an expansion coefficient  $B_a^\alpha$  [29]

$$B_a^\alpha = \sum_{Nn_z\Sigma} C_{l\Lambda \frac{1}{2}\Sigma}^{j\Omega_\alpha} A_{Nn_z\Lambda}^{N0l} b_{Nn_z\Sigma}, \quad A_{Nn_z\Lambda}^{N0l} = \langle N0l\Lambda | Nn_z\Lambda \rangle. \quad (6)$$

Detailed formulas used for the coefficient  $B_a^\alpha$  and the overlap integral  $A_{Nn_z\Lambda}^{N0l}$  are presented in Appendix B. The  $T = 0$  pairing contribution is included as an imaginary term in the  $np$  pairing potential in Eq. (5).  $K$  is a projection number of a total angular momentum  $J$  onto the  $z$  axis and selected as  $K = 0$ . The Brueckner  $G(aaccJT)$  matrix represents the state-dependent pairing matrix element (PME) calculated in the spherical basis. In this work, in order to study nuclear structure effects on the pairing potentials, we exploit a constant two-body PME in line with the Kisslinger-Sorensen approach [35,44], i.e., the innermost square brackets in Eqs. (4) and (5) are treated as a constant, and compare to the results by the state-dependent Brueckner  $G$ -matrix PME. We sum up all possible  $J$  values of the coupling of two-particle state assigned by ( $aa$ ) or ( $cc$ ) in the spherical basis, which has the  $K = 0$  projection. This sum of  $J$  values is due to the expansion of the deformed state by the spherical states ( $aa$ ) or ( $cc$ ).  $\Delta_{\alpha n\bar{a}n}$  is obtained from Eq. (4) by replacing  $p$  by  $n$ .

### III. RESULTS AND DISCUSSIONS

This study exploits a cylindrical Woods-Saxon potential with the Blomqvist and Wahlborn parameter set reported by Cwiok *et al.* [45]. In this parameter set, radius parameters of

a central and a spin-orbit (SO) potential and strength of the SO potential of neutrons are the same as those of protons. So we can argue possible charge symmetry breaking effect on the like- and unlike-pairing gaps due to the Coulomb force. The particle model space for all nuclei considered here was extended to  $N = 5\hbar\omega$  for a deformed basis, which was expanded up to  $N_0 = 10\hbar\omega$  in a spherical basis.

In this work, we switch on and off the Coulomb and/or the SO interaction, respectively, in the deformed WS (DWS) potential. Consequently, we may examine the Wigner spin-isospin SU(4) symmetry, in which the nuclear Hamiltonian satisfies the following relation:

$$[H, \Sigma_i \tau_i] = [H, \Sigma_i \sigma_i] = [H, \Sigma_i \tau_i \sigma_i] = 0. \quad (7)$$

The SU(4) symmetry is usually broken either by  $\tau_i$  term in the Coulomb interaction or by the  $\sigma_i$  term in the SO interaction. The SU(4) symmetry is also broken if a repulsive proton-proton ( $pp$ ) Coulomb interaction on the pairing correlations is taken into account in the residual interaction.

In the following, we take two  $N = Z$  nuclei,  $^{24}\text{Mg}$  and  $^{36}\text{Ar}$  for  $sd$ -shell,  $^{48}\text{Cr}$  and  $^{64}\text{Ge}$  for  $pf$ -shell, and  $^{108}\text{Xe}$  and  $^{128}\text{Gd}$  for  $sdg_{7/2}h_{11/2}$ -shell nuclei for the study of the Coulomb and the SO force. We calculate the like-pairing ( $nn$  and  $pp$ ) and the unlike-pairing ( $np$ ) gaps with full terms in the DWS potential, and study the role of each potential on the pairing gaps.

In actual calculation, we calculate the quasiparticle energy for each  $\alpha$  state,  $E_\alpha^{qp} = \sqrt{(\epsilon_\alpha - \lambda_\alpha)^2 + \Delta_\alpha^2}$ , with its SPS energy  $\epsilon_\alpha$  obtained by the DWS potential and chemical potential  $\lambda_\alpha$  by the iteration for conserving particle numbers in average. And then we take the lowest quasiparticle energy in the state  $\alpha$  and adopt the  $\Delta_{p\bar{p}\alpha}$  as the pairing gap  $\Delta_p$  to be compared with

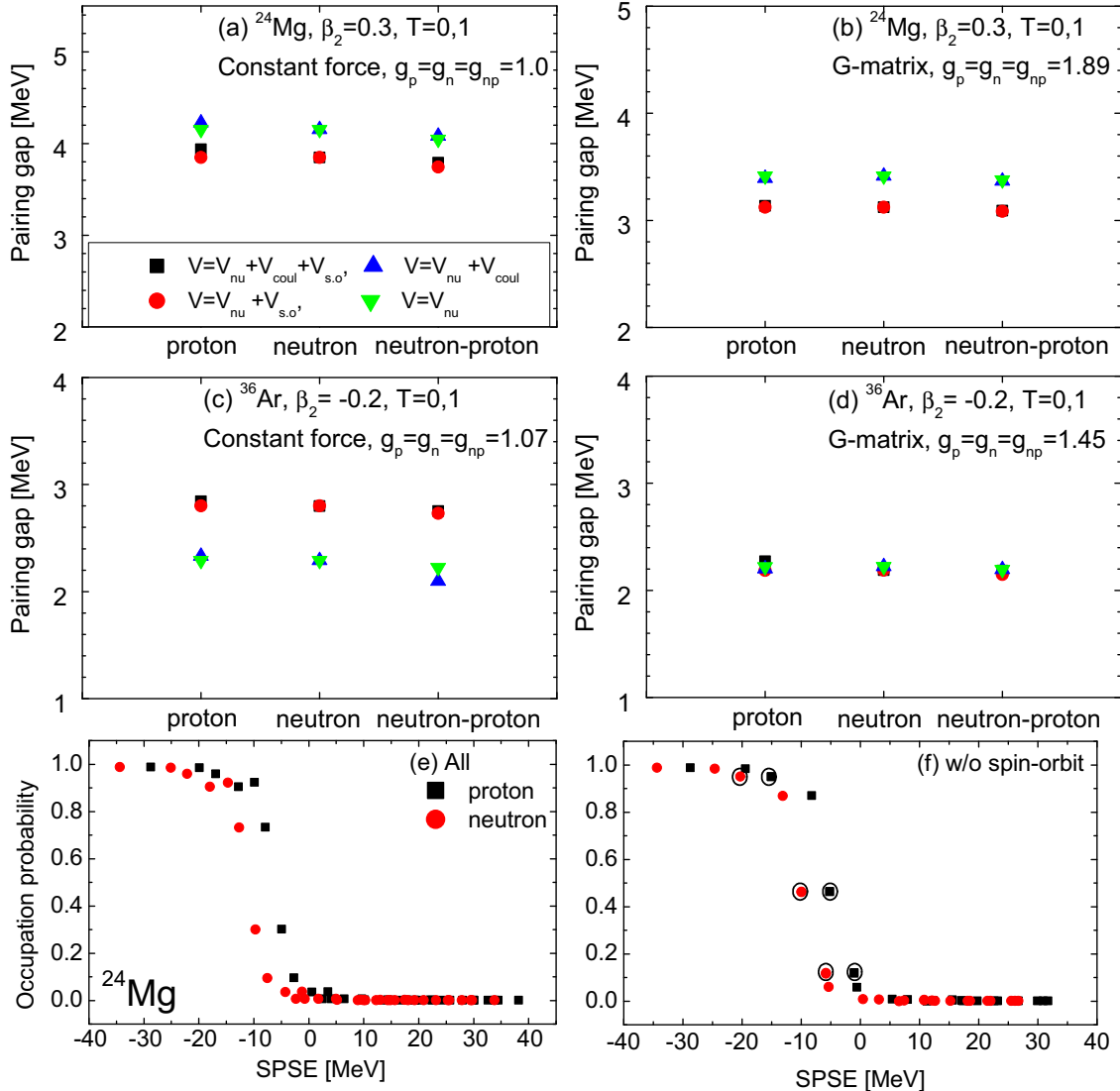


FIG. 1. Pairing gaps of  $pp$ ,  $nn$  and  $np$  for the  $sd$ -shell nuclei,  $^{24}\text{Mg}$  and  $^{36}\text{Ar}$ , by the DBCS model based on a deformed Woods-Saxon potential [45]. Black squares (red circles) are calculated with  $V_{\text{nuc1}}(\equiv V_{\text{nu}}) + V_{\text{coul}} + V_{\text{s.o.}}(V_{\text{nu}} + V_{\text{s.o.}})$  and blue triangles (green inverted triangles) for  $V_{\text{nu}} + V_{\text{coul}}(V_{\text{nu}})$ . The pairing gaps are calculated by two different PME cases. (a) and (c) are by the constant PME, and (b) and (d) are by the state-dependent  $G$ -matrix PME. (a) and (b) are for  $^{24}\text{Mg}$  and (c) and (d) are for  $^{36}\text{Ar}$ . (e) and (f) represent the occupation probabilities of protons and neutrons with and without the SO force as a function of single particle energy with the  $G$ -matrix PME for  $^{24}\text{Mg}$ . The circles and squares surrounded by black circles in (f) imply the existence of degenerated states.

the odd-even mass difference. In the process, by changing the strength parameter  $g_{pp}(=g_p)$  in Eq. (4), which is a kind of renormalization constant due to a finite Hilbert particle model space, we fit the pairing gap to the empirical pairing gap in Table I. Other strength parameters,  $g_{nn}(=g_n)$  and  $g_{np}^{T=0,1}$ , are adopted as the same as the  $g_{pp}$  value for each nucleus because we have interests only on the variations of the pairing gaps by the SU(4) symmetry breaking. The  $np$  pairing gaps in Figs. 1, 3, 5, and 7 show the absolute value of the complex  $\Delta_{np}$  given by Eq. (5).

For the constant PME, we take an arbitrary value close to 1.0 for the strength parameter, so that the calculated gap energies with the constant PME have no meaning quantitatively. Deformation parameters  $\beta_2$  are determined at the minimum ground-state energies [32,33].

### 1. $^{24}\text{Mg}$ and $^{36}\text{Ar}$

In Figs. 1(a)–1(d), we present the pairing gaps  $\Delta_p$ ,  $\Delta_n$ ,  $\Delta_{np}$  obtained from the lowest quasiparticle energy state near Fermi surface. All like- and unlike-pairing gaps for  $^{24}\text{Mg}$  and  $^{36}\text{Ar}$  are very close and independent to the given potential types. It means that the charge independence symmetry is mostly conserved for the  $sd$ -shell  $N=Z$  nuclei.

We look into details of the results in Figs. 1(a)–1(d). First, we note that the differences between triangles and inverted triangles and between squares and circles are very small. It implies that all pairing gaps are not affected by the Coulomb interaction, regardless of the existence of the SO potential. It can be easily understood if we notice the following facts: The Coulomb potential considered here is a component in

the mean field and induces only a Coulomb energy difference between neutrons and protons. But the pairing gaps stem from the residual interactions. As a result, they are not affected by the Coulomb interaction.

Second, the unlike-pairing gap is almost equal to the like-pairing gaps. The Coulomb energy difference is believed to produce the smaller  $np$  pairing with the heavier (neutron-rich) nuclei. But, in light nuclei, the Coulomb energy difference does not suppress the  $np$  pairing gap even if we use the state-dependent PME. It implies that the Coulomb energy difference does not seriously affect the pairing correlations, at least for  $sd$ -shell  $N = Z$  nuclei.

However, in heavy nuclei, the SPS reordering by the central Coulomb interaction appears and affects the pairing correlations. The repulsive Coulomb interaction among protons may also contribute to the residual interactions. Recent calculation of diproton correlations in proton-rich light nuclei could be an interesting suggestion for this kind of  $pp$  pairing correlations [46]. It is pointed out that the two-body Coulomb potential decreases the pairing matrix elements by about 10%. In the present approach, we do not include the repulsive residual Coulomb interaction among protons.

Third, the SO force influences the pairing gaps, as we note the differences between top and bottom results in Figs. 1(a)–1(c). The SO force decreases the pairing gaps for  $^{24}\text{Mg}$  as shown in Figs. 1(a) and 1(b). It comes from the fact that the number of the pairs (see Eq. (12) in Ref. [6]) are decreased by the SO splitting. This tendency by the SO force is closely related to the smearing of the SPS occupation probabilities

as shown in Figs. 1(e) and 1(f). If we switch on the SO force, the smearing becomes small as shown in Fig. 1(e). Note that the circles in Fig. 1(f) mean degenerated states, which affect the smearing.

The evolution of SPSs for  $^{24}\text{Mg}$  by the deformation parameter  $\beta_2$  is illustrated in Fig. 2 for the case (a) with and (b) without the SO force, respectively. In Fig. 2(b), many degenerated states appear in the absence of the SO force, which keep more particles around Fermi surface and make the larger pairing gaps leading to the larger smearing as shown in Fig. 1(f). In Fig. 2(a), by the SO force in the prolate deformation the  $0d_{3/2}$  shell is split above Fermi surface, while the  $0d_{5/2}$  shell splitting still remains around Fermi surface for  $^{24}\text{Mg}$ . As a result, the pairing gaps are reduced, which is closely related with the small smearing by the SO force in Fig. 1(e).

But, for  $^{36}\text{Ar}$  case, the SO force affects differently. That is, it increases the pairing gaps as shown in Fig. 1(c) because of the following reasons. The SO force splits the  $0d$  shell and makes the smearing small by the splitting of the  $0d_{3/2}$  shell in a similar way to  $^{24}\text{Mg}$  case, but the  $7/2_1^-$  state in the  $0f_{7/2}$  shell in the oblate deformation region increases its occupation probability because of the intruder configuration in the  $sd$  orbits as shown in Fig. 2(a). As a result, the pairing gap becomes larger. But its magnitude depends on the PME as shown in Fig. 1(d).

Here we present matrix elements by the SO interaction in the Nilsson oscillator basis for diagonal and off-diagonal cases as follows [47]:

$$\begin{aligned} \langle n_z, n_\perp, \Lambda, \Sigma | \vec{l} \cdot \vec{s} | n_z, n_\perp, \Lambda, \Sigma \rangle &= \Lambda \Sigma, \\ \langle n_z + 1, n_\perp - 1, \Lambda + 1, \Sigma - 1 | \vec{l} \cdot \vec{s} | n_z, n_\perp, \Lambda, \Sigma \rangle &= \frac{1}{2} [(n_z + 1)(n_\perp - \Lambda)]^{1/2}, \\ \langle n_z + 1, n_\perp - 1, \Lambda - 1, \Sigma + 1 | \vec{l} \cdot \vec{s} | n_z, n_\perp, \Lambda, \Sigma \rangle &= -\frac{1}{2} [(n_z + 1)(n_\perp + \Lambda)]^{1/2}, \\ \langle n_z - 1, n_\perp + 1, \Lambda - 1, \Sigma + 1 | \vec{l} \cdot \vec{s} | n_z, n_\perp, \Lambda, \Sigma \rangle &= \frac{1}{2} [n_z(n_\perp - \Lambda + 2)]^{1/2}, \\ \langle n_z - 1, n_\perp + 1, \Lambda + 1, \Sigma - 1 | \vec{l} \cdot \vec{s} | n_z, n_\perp, \Lambda, \Sigma \rangle &= -\frac{1}{2} [n_z(n_\perp + \Lambda + 2)]^{1/2}, \end{aligned} \quad (8)$$

where the vector  $\vec{l}$  is the Nilsson's stretched angular momentum vector. The matrix elements of the SO interaction in Eq. (8) are independent of the deformation parameter  $\beta_2$ . But, the SO potential in the DWS potential has a surface-peaked structure. Consequently, the SO splitting can be affected by the deformation through this radial dependence. In fact, Fig. 2(a) reveals that the splitting becomes larger with the deformation. On top of that, the deformation can split the SPS as follows:

$$\epsilon_0(n_z, n_\perp, m_l) \simeq \hbar\omega_0(\delta) \left[ \left( N + \frac{3}{2} \right) + \delta \left( \frac{N}{3} - n_z \right) \right], \quad (9)$$

where  $\delta$  is related to the deformation parameter  $\beta_2 \sim (2/3)\sqrt{4\pi/5}\delta$ . Figure 2(b) clearly shows the deformation splitting. Therefore, the splitting of SPS energies occurs by the deformation in Eq. (9) as well as by the SO force due to

the potential dependent factor, and seriously affect the pairing correlation.

Here, we make a short summary about the SO force effect as follows. By the splitting, the pairing gaps become smaller, as in  $^{24}\text{Mg}$  case, and the smearing decreases. But, the deformation splitting in Eq. (9) might be as important as the SO splitting because it may bring about the intruder, which increases the smearing and consequently gives rise to the larger pairing, as in  $^{36}\text{Ar}$  case.

For  $^{36}\text{Ar}$ , the SO force does not change the pairing gaps for the state-dependent PME in Fig. 1(d). This might be due to the fact that the Brueckner  $G$  matrix has different properties of the intruder state in the competition between the SO force and the deformation effect. Finally, if we switch off the Coulomb and the SO interaction, the SU(4) symmetry is shown to be almost hold on the pairing gaps, as shown in the green inverted triangles.

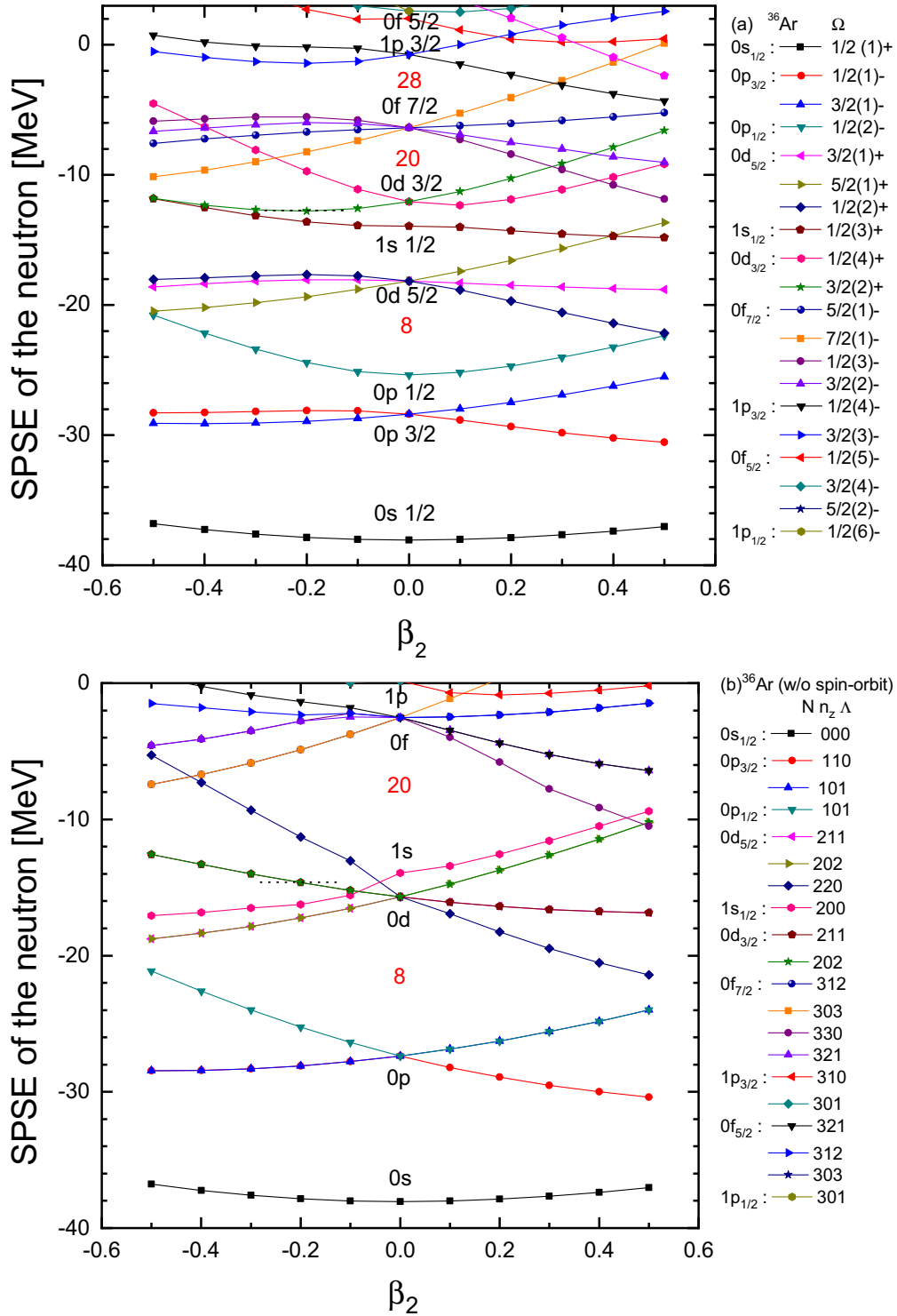
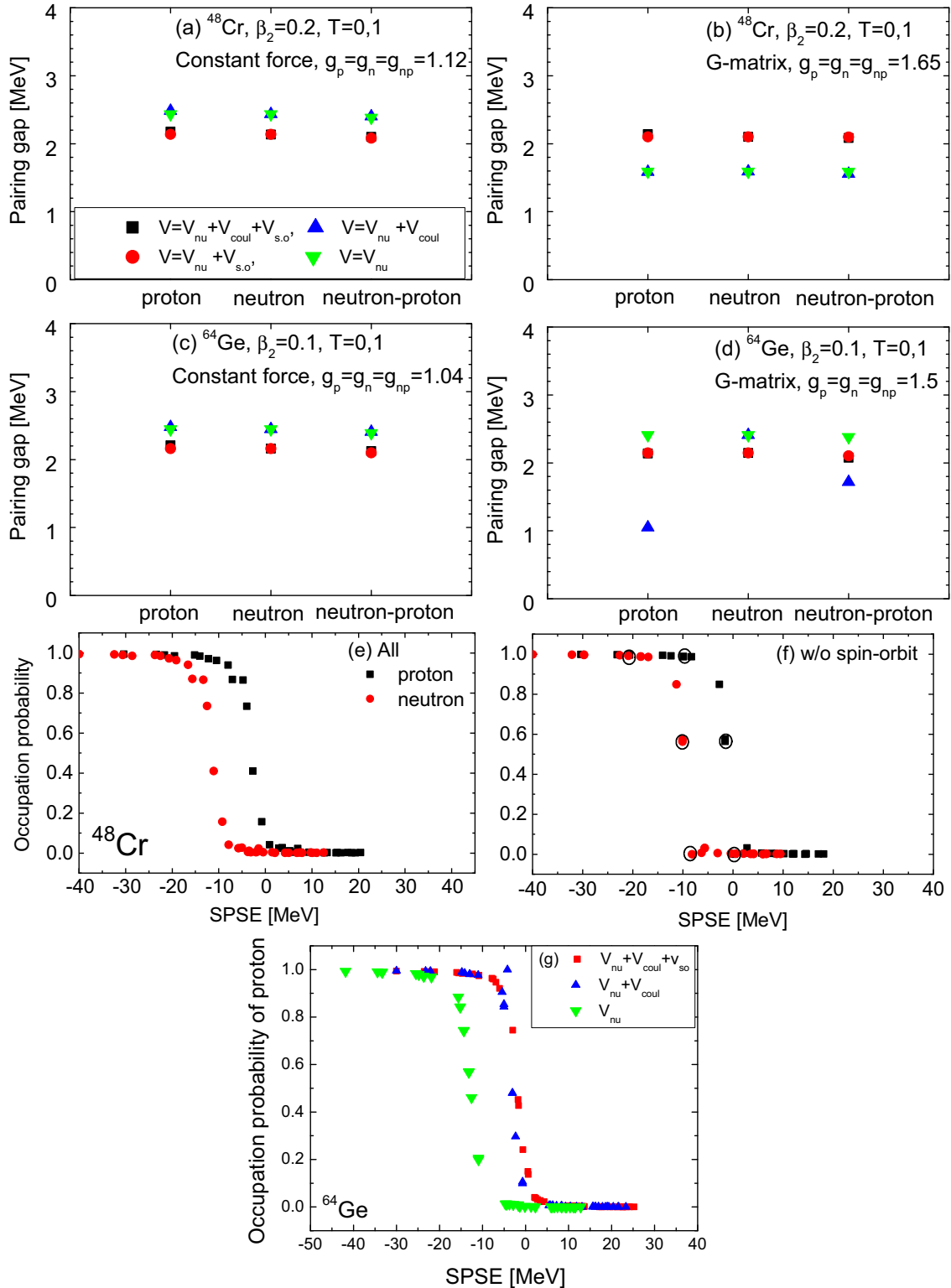


FIG. 2. The SPSE of neutrons for  $^{36}\text{Ar}$  as a function of deformation parameter  $\beta_2$ . (a) is calculated with  $V_{\text{nucl}} + V_{\text{coul}} + V_{\text{s.o.}}$ , and (b) is with  $V_{\text{nucl}} + V_{\text{coul}}$ , i.e., without the SO force. The black dotted lines denote Fermi energy. Some of the states in (b) are degenerated.

### 2. $^{48}\text{Cr}$ and $^{64}\text{Ge}$

Results for *pf*-shell nuclei,  $^{48}\text{Cr}$  and  $^{64}\text{Ge}$ , are shown in Fig. 3 with the shell evolution in Fig. 4. First, one finds that the Coulomb effect is similar to that of the *sd*-shell nuclei. Namely, the Coulomb effect does not influ-

ence on the pairing gaps. But, interestingly, the Coulomb effect for  $^{64}\text{Ge}$  appears appreciably for the state-dependent PME, that is, it splits the proton and the *np* pairings as shown in the green and blue triangles in Fig. 3(d), if we switch off the SO force. The downward splitting

FIG. 3. The same as Fig. 1, but for  $pf$  shell  $^{48}\text{Cr}$  and  $^{64}\text{Ge}$ .

of the pairing gaps might stem from the reordering of SPSs due to the degeneracies in the absence of the SO force.

Results in Fig. 3(g) show the proton smearing for each potential case. This smearing is closely associated with the

proton pairing gaps, i.e., the larger pairing gaps in Fig. 3(d) induce the larger smearing. For instance, the smearing disappears by the  $V_{coul}$  term, which is related to the decrease of the proton pairing gap denoted as a blue triangle in Fig. 3(d).

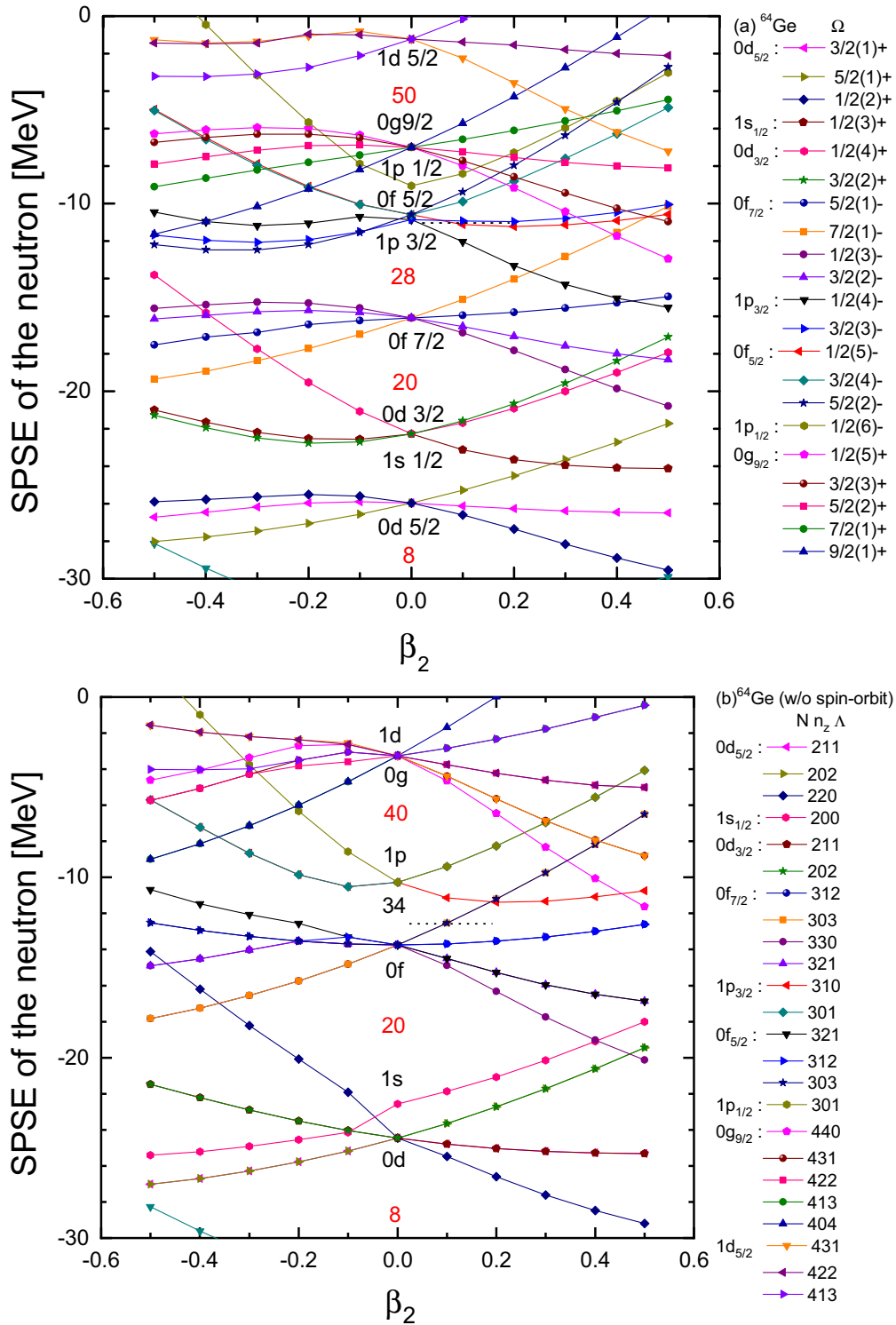


FIG. 4. Same as Fig. 2, but for  $^{64}\text{Ge}$ .

Second, in Figs. 3(a) and 3(c), the SO force decreases the pairing gaps for the constant PME. It can be inferred by the smearing features of the SPS for  $^{48}\text{Cr}$  and  $^{64}\text{Ge}$  in Figs. 3(e) and 3(f). But the state-dependent PME in Fig. 3(b) increases the pairing for  $^{48}\text{Cr}$  case with the SO force. It may come from a peculiar circumstance of the level density and Pauli blocking near the Fermi surface of  $^{48}\text{Cr}$ .

In principle, the SO force may have some contributions from the Coulomb force. The SO force in the present DWS potential has a factor related to the Coulomb force given in a derivative form, which gives rise to different proton and neutron splitting. But, in the present work, we turn off the Coulomb contribution in the SO force in order to study the Wigner SU(4) symmetry, so that the same SO forces are

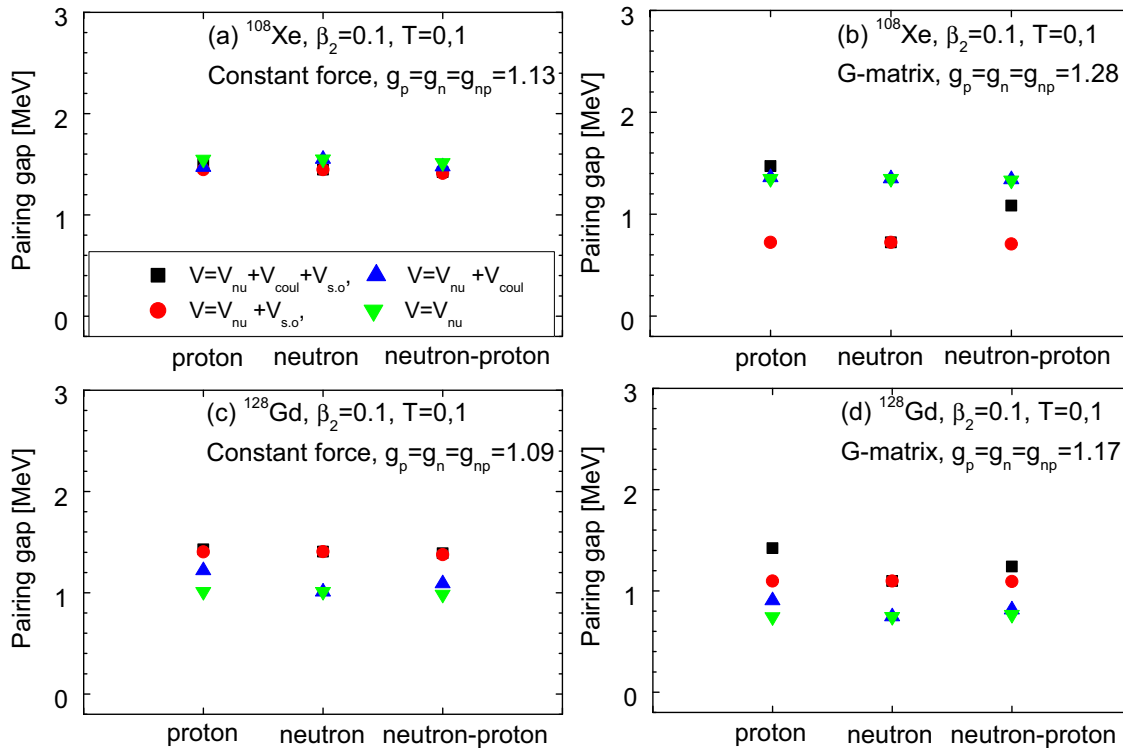


FIG. 5. The same as Fig. 1, but for  $sdg_{7/2}h_{11/2}$ -shell nuclei,  $^{108}\text{Xe}$  and  $^{128}\text{Gd}$ .

used for protons and neutrons. Test calculations including the Coulomb factor in the SO force show that the Coulomb force contribution is not large enough to change the pairing gaps.

### 3. $^{108}\text{Xe}$ and $^{128}\text{Gd}$

Finally, we discuss two heavy nuclei in  $sdg_{7/2}h_{11/2}$ -shell  $N = Z$  nuclei in Fig. 5, whose nuclei were reported to have strong IS ( $T = 0$ ) pairing correlations [11]. Since these nuclei have strong Coulomb effects in the mean field, we examine carefully the Coulomb effect. Evolutions of SPSs by the deformation parameter  $\beta_2$  for  $^{128}\text{Gd}$  are shown in Fig. 6, where we compare the SPS evolution [Fig. 6(a)] with and [Fig. 6(b)] without the Coulomb interaction.

One can find reordering of the  $sdgh$  shell near Fermi surface by the Coulomb interaction, which causes large Coulomb effects on the pairing correlations. The states in the  $1d_{5/2}$  shell are almost overlapped with those in the  $0h_{11/2}$  shell by the Coulomb force as shown in Fig. 6(a), which makes the smearing larger. As a result, the proton and the  $np$  pairing gaps are expected to increase by the Coulomb force. But, the SO force decreases (increases) the pairing gaps for the case without (with) the existence of the intruder as argued in the  $sd$ - and  $pf$ -shell nuclei.

Therefore there appears the competition of the Coulomb and the SO force in the  $sdgh$ -shell nuclei. For example, for  $^{108}\text{Xe}$  the SO force decreases the pairing gaps. In particular, the SO force decreases largely the neutron pairing gap for the state-dependent PME in Fig. 5(b) because of the  $0g$  shell degeneracy. But the proton and the  $np$  pairing gap are increased by the Coulomb force if we note that the red circles move to the black squares by the Coulomb force. This separation

by the Coulomb force does not take place in the  $sd$ - and  $pf$ -shell nuclei. For  $^{128}\text{Gd}$ , the SO force increases the neutron pairing gap due to the intruder of  $0h_{11/2}$  shell. The Coulomb force enlarges much more the  $np$  and the proton pairing gap increased by the SO force as shown in Figs. 5(c) and 5(d).

### 4. Competition of isoscalar and isovector interactions

The last discussion is the isoscalar (IS) pair condensation. In a previous paper [32], we argued that the IS condensation may happen in  $^{24}\text{Mg}$  with  $\beta_2 = 0.4$  deformation (see Fig. 3 in Ref. [32]). Therefore, we show the results of the pairing gap by two different deformations  $\beta_2 = 0.3$  and  $0.4$  in Figs. 7(a) and 7(b), respectively, and also present the  $np$  pairing gaps obtained by the three times enhanced  $T = 0$  pairing strength,  $g_{np}^{T=0} = 3.0 \times g_{np}^{T=1}$ , in the last column (denoted as  $np^*$ ). This enhancement strength is explained in Eq. (A2) in Appendix A. Similar calculations for the  $pf$ - and  $sdgh$ -shell cases are done for  $^{48}\text{Cr}$  and  $^{108}\text{Xe}$  in Figs. 7(c)–7(f). Here the  $\beta_2$  values in the left panels are from the  $\beta_2^{\text{ours}}$  in Table I, while the values in the right panels are taken to be a bit larger than the  $\beta_2^{\text{ours}}$  by considering the  $|\beta_2^{E2}|$  in Table I.

We note two interesting points. One is the results of the enhanced  $T = 0$  case in the last column. They illustrate large SO effects compared to the normal  $T = 0$  case. It implies that the stronger IS  $np$  pairing would lead to the more degenerated states in the absence of the SO interaction. But detailed features depend on the shell evolution by the deformation as shown in Figs. 7(c) and 7(f).

Another interesting point is that the  $np$  pairing gaps are not changed even by the enhanced IS pairing in the small deformation region as shown in the left panels, but they

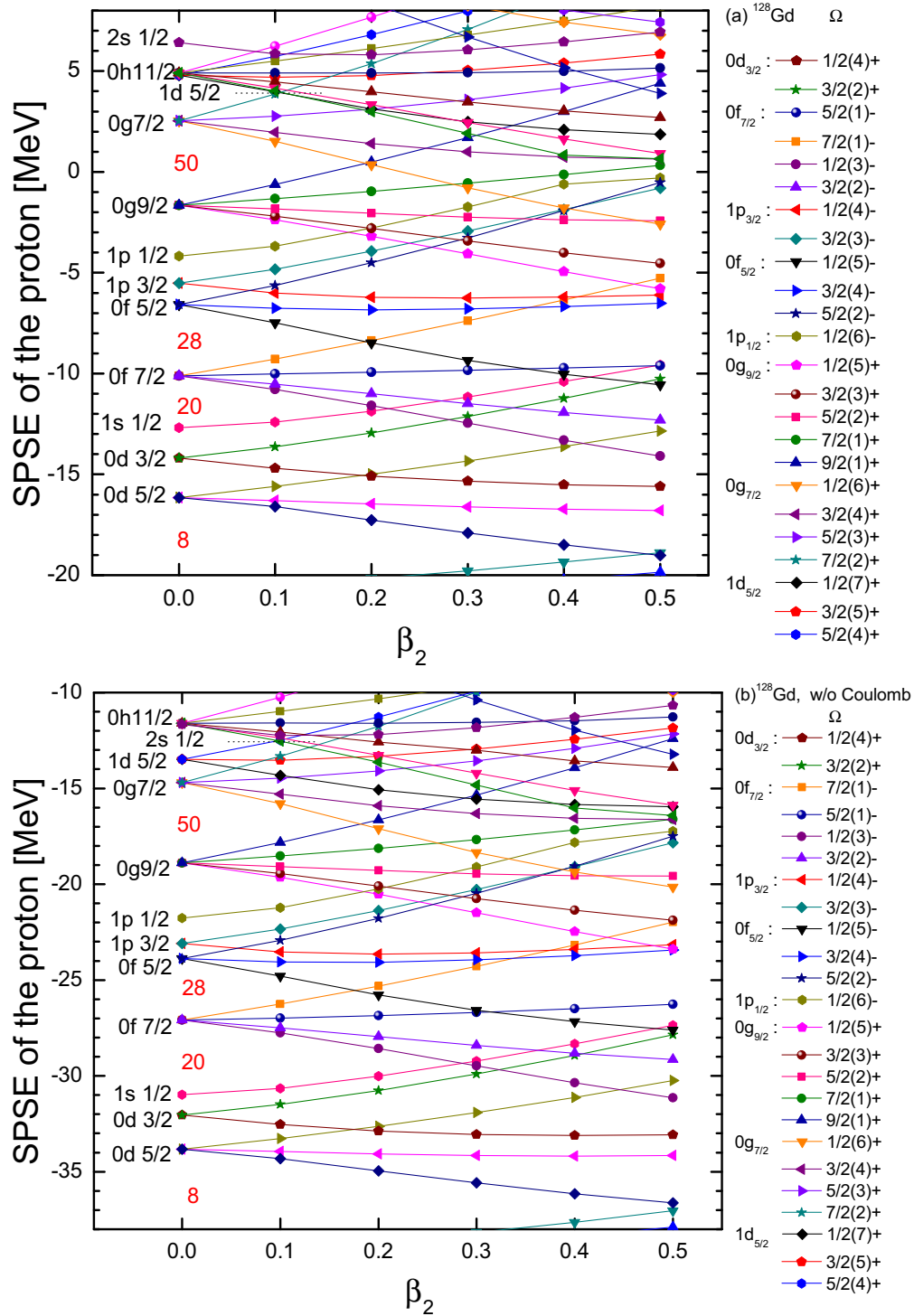


FIG. 6. The SPS energies of proton for  $^{128}\text{Gd}$  as a function of deformation parameter  $\beta_2$ . (a) is calculated with  $V_{\text{nucl}} + V_{\text{coul}} + V_{\text{s.o.}}$ , and (b) is for  $V_{\text{nucl}} + V_{\text{s.o.}}$  (without Coulomb force). The black dotted lines denote Fermi energy.

increase in the larger deformation in the right panels. One infers that the IS pairing can dominate the  $np$  pairing gap with the larger deformation region. This tendency is clearly illustrated in Fig. 8. We present ratios of the IV and IS pairing gap contributions to the  $np$  pairing gap along the deformation with the enhanced IS pairing. For  $^{24}\text{Mg}$  in Fig. 8(a), the  $\beta_2 = 0.1 \approx 0.3$  region is dominated by the IV contribution,

while for  $\beta_2 \approx 0.4$  region the  $np$  pairing gap is dominated by the IS contribution. That is, a phase transition from IV to IS dominance occurs in the region from  $\beta_2 = 0.3$  to  $\beta_2 = 0.4$ , as argued in our previous paper [32]. This transition is termed as the IS pair condensation in the present work. If we take the normal IS pairing interaction, the IV contribution dominates the  $np$  pairing gap all the way.

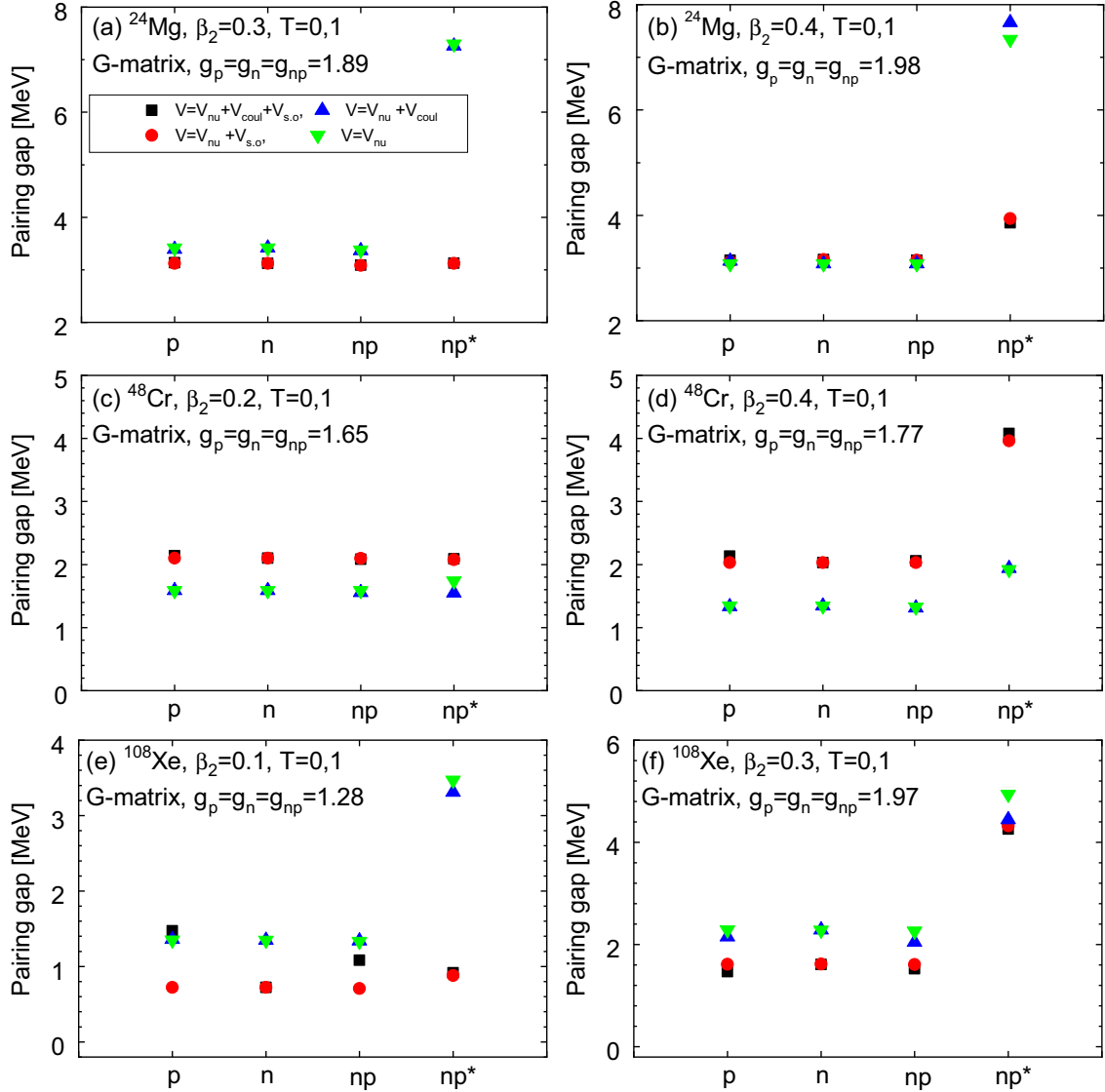


FIG. 7. Same as Fig. 1, but the last column shows the  $np$  pairing gap by the three times enhanced  $T = 0$  pairing strength denoted as  $np^*$ . (a) and (b) for  $^{24}\text{Mg}$  are obtained by  $\beta_2 = 0.3$  and  $0.4$  case, respectively. (c) and (d) for  $^{48}\text{Cr}$  are by  $\beta_2 = 0.2$  and  $0.4$  case, respectively. (e) and (f) for  $^{108}\text{Xe}$  are by  $\beta_2 = 0.1$  and  $0.3$  case, respectively. Pairing strengths  $g_p$  are fixed to reproduce the empirical proton pairing gaps and others are kept to have the same values as  $g_p$  similarly to Fig. 1.

This trend also appears for  $^{48}\text{Cr}$  in Fig. 8(b): IS contribution dominates the  $np$  pairing gap, if we increase the deformation with the enhanced IS pairing interaction. For  $^{108}\text{Xe}$ , even the normal IS pairing shows such a phase transition feature in Fig. 8(d). If we take the enhanced IS pairing, the  $np$  pairing gap of  $^{108}\text{Xe}$  is always dominated by the IS contribution as shown in Fig. 8(c). It implies that  $N = Z$  heavy nuclei may have the IS condensation by the normal IS pairing if they are largely deformed, according to our calculation. If we adopt the enhanced IS pairing interaction for  $^{108}\text{Xe}$ , the IS pairing interaction becomes dominant for all deformation region as shown in Fig. 8(c).

Therefore we can conjecture that the stronger deformation may give rise to the IS condensation through a phase transition. For example, in this work, the deformation pa-

rameters  $\beta_2$  in Figs. 7(a), 7(c) and 7(e) are taken from our theoretical model, DBCS approach. Results by these deformations in Fig. 8 show only IV dominance even with the enhanced  $T = 0$  pairing. But the values near experimental deformation  $|\beta_2^{E2}|$  for  $^{24}\text{Mg}$  and  $^{48}\text{Cr}$  in Table I give rise to the IS pair condensations explicitly. Future calculations including  $\beta_3$  and triaxial deformation adjacent to the data are desirable for further conclusive arguments for the IS pair condensation.

#### IV. CONCLUSION

In conclusion, we studied the SO interaction and the Coulomb effects on the like- and unlike-pairing correlations in  $sd$ -,  $pf$ -, and  $sdg_{7/2}h_{11/2}$ - shell  $N = Z$  nuclei. The SPS

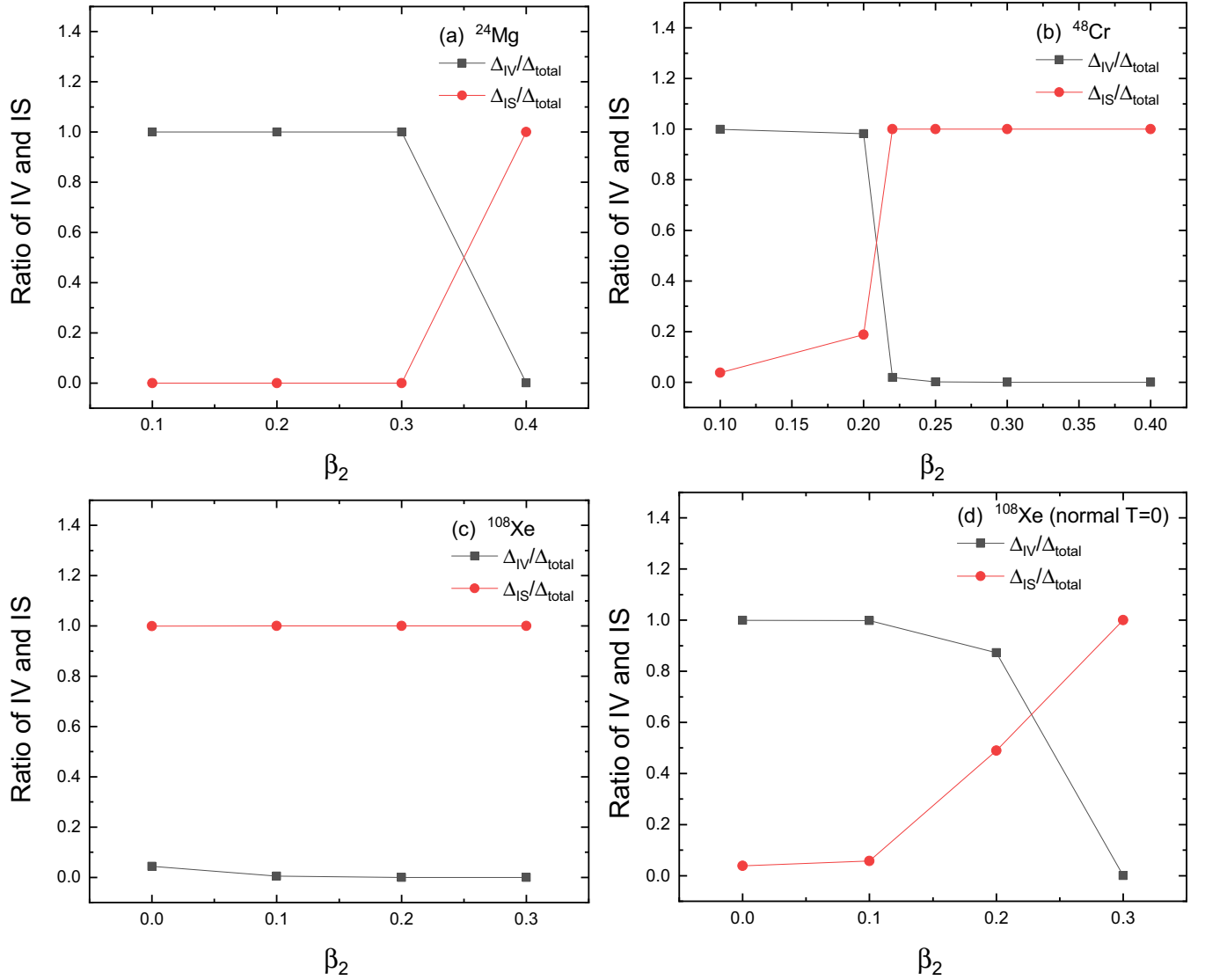


FIG. 8. Ratio of IV and IS pairing interaction gap to the total  $np$  pairing gap by the enhanced  $T = 0$  pairing [(a)–(c)] in Eq. (A2) for  $^{24}\text{Mg}$ ,  $^{48}\text{Cr}$ , and  $^{108}\text{Xe}$ , respectively. For  $^{108}\text{Xe}$ , we showed two cases, enhanced (c) and normal (d)  $T = 0$  pairing.

energies are calculated by a deformed WS potential. In order to investigate the pairing gaps by the like- and unlike-pairing correlations, we exploit two pairing interactions: the constant and the state-dependent Brueckner  $G$ -matrix PME. The results by the constant PME show the Coulomb and SO force effects similar to those by the state-dependent PME in most cases, but show large differences in several cases compared to the pairing gaps by the state-dependent PME. It comes from the fact that the results calculated with the state-dependent PME are very sensitive to the energy splitting by both the deformation and the SO force in the mean-field level as well as some characteristics of each orbital state, as shown in  $^{48}\text{Cr}$  case.

The SO and the Coulomb force, which can break explicitly the Wigner SU(4) symmetry, are shown to change substantially the pairing gaps. Namely, the SO force splits the degeneracy of shell orbits and generally decreases the pairing gaps, which brings simultaneously the decrease of

the number of the pairs. However it depends largely on the location of Fermi surface and the deformation. That is, some intruder states come into near the Fermi surface in the case of large deformation and increase the pairing gaps inducing more smearing.

The Coulomb interaction does not affect the pairing gaps at least for  $sd$ -shell nuclei. But its effect appears for  $pf$ - and  $sdg_{7/2}h_{11/2}$ -shell nuclei because of the proton SPS reordering by the Coulomb interaction. For heavy nuclei, the Coulomb effect can be more important than the SO force. The Wigner SU(4) symmetry on the pairing correlations appears explicitly in the limit of strong pairing force, but the symmetry is broken by the Coulomb and the SO interaction in the realistic cases.

Finally, we argued that the IS pair condensation may occur in deformed  $N = Z$  nuclei, such as  $^{24}\text{Mg}$  and  $^{48}\text{Cr}$ , through an abrupt phase transition from IV to IS interaction due to the enhanced  $T = 0$   $np$  pairing correlations. For heavy nuclei

such as  $^{108}\text{Xe}$ , the transition may happen more smoothly even with the normal  $T = 0$  pairing interaction. More detailed and systematic calculations regarding the IS pair condensation and the coexistence of the IV and IS phase for heavy  $N \simeq Z$  nuclei are in progress.

### ACKNOWLEDGMENTS

This work was supported by the National Research Foundation of Korea (Grants No. NRF-2018R1D1A1B05048026, No. NRF-2017R1E1A1A01074023, and No. NRF-2013M7A1A1075764).

### APPENDIX A: ENHANCED ISOSCALAR PAIRING STRENGTH

In the present DBCS framework, we include only  $n\bar{p}$  and  $\bar{n}p$  pairing correlations for the unlike pairing by the  $np$  pairing correlations. But we may effectively include the  $T = 0$  contributions due to the  $np$  and  $\bar{n}\bar{p}$  channels by multiplying a factor 2 to the  $T = 0$  pairing matrices by the  $n\bar{p}$  and  $\bar{n}p$  pairs [32]. This has been done by following Ref. [3], which took into account the  $np$ ,  $\bar{n}\bar{p}$ ,  $\bar{n}p$ , and  $n\bar{p}$  pairings. If we assume

$$\begin{aligned} \langle \alpha n \alpha p, T = 0 | V_{\text{pair}} | \beta n \beta p, T = 0 \rangle \\ = \langle \alpha n \alpha p, T = 0 | V_{\text{pair}} | \bar{\beta} n \bar{\beta} p, T = 0 \rangle, \end{aligned} \quad (\text{A1})$$

then  $\text{Im} \Delta_{\alpha n \alpha p}^{T=0} = 0$  and  $\text{Re} \Delta_{\alpha n \alpha p}^{T=0} = \text{Im} \Delta_{\alpha n \bar{\alpha} p}^{T=0}$  by Eqs. (5)–(7) in Ref. [3]. It leads to

$$|\Delta_{n p \alpha}^{T=0}|^2 = 2|\Delta_{\alpha p \bar{\alpha} n}^{T=0}|^2 + 2|\Delta_{\alpha p \alpha n}^{T=0}|^2 = 4|\Delta_{\alpha p \bar{\alpha} n}^{T=0}|^2, \quad (\text{A2})$$

where the factor 2 in the second equality comes from the  $\bar{\alpha} p \alpha n$  and  $\bar{\alpha} p \bar{\alpha} n$  pairing, respectively. Consequently, we multiply a weighting factor  $1.5 \times 2 = 3.0$  to the  $T = 0$  pairing  $G$ -matrix strength [32]. This is the enhanced IS pairing used in the last column of Figs. 7 and 8. The factor 1.5 is employed to take into account the IV quenching (or IS enhancement) of the M1 spin strength data at Ref. [20].

### APPENDIX B: EXPANSION OF A DEFORMED WAVE FUNCTION BY A SPHERICAL WAVE FUNCTION

We denote a spherical harmonic oscillator (HO) wave function as

$$|N_0 l \Lambda_\alpha \rangle |\Sigma\rangle = \sum_j C_{l \Lambda_\alpha \frac{1}{2} \Sigma}^{j \Omega_\alpha} |N_0 l j \Omega_\alpha \rangle, \quad (\text{B1})$$

where  $C_{l \Lambda_\alpha \frac{1}{2} \Sigma}^{j \Omega_\alpha}$  is a Clebsch-Gordan coefficient for a coupling of an orbital ( $l$ ) with its projection  $\Lambda_\alpha$  and a spin angular momentum ( $\frac{1}{2}$ ) with its projection  $\Sigma$  to a projection  $\Omega_\alpha$  of a total angular momentum ( $j$ ) defined as  $\Omega_\alpha = \Lambda_\alpha + \Sigma$ .

Then a deformed HO wave function  $|N n_z \Lambda_\alpha \Omega_\alpha \rangle (= |\Lambda_\alpha + \Sigma\rangle) = |N n_z \Lambda_\alpha \rangle |\Sigma\rangle$  can be expanded in terms of the spherical HO wave function  $|N_0 l \Lambda_\alpha \rangle |\Sigma\rangle$  in Eq. (B1) as follows:

$$|N n_z \Lambda_\alpha \rangle |\Sigma\rangle = \sum_{N_0=N, N \pm 2, N \pm 4, \dots} \sum_{l=N_0, N_0-2, N_0-4, \dots} A_{N n_z \Lambda}^{N_0 l, (n_r = \frac{N_0-l}{2})} |N_0 l \Lambda_\alpha \rangle |\Sigma\rangle, \quad (\text{B2})$$

where a major quantum number  $N_0$  is given as  $N_0 = 2n_r + l$  with a radial quantum number  $n_r$  in a spherical basis. The major shell quantum number  $N$  in a deformed basis is given as  $N = n_x + n_y + n_z = n_\perp + n_z$  with  $2n_\rho + \Lambda = n_\perp$ . The spatial overlap integral  $A_{N n_z \Lambda}^{N_0 l} = \langle N_0(n_r) l \Lambda | N(n_\rho) n_z \Lambda \rangle$  is calculated numerically in a spherical coordinate system as follows:

$$\begin{aligned} A_{N n_z \Lambda}^{N_0 l} = \int dV' \left[ \left[ \frac{2(n_r!)}{\Gamma(n_r + l + 3/2)} \right]^{1/2} (b_s)^{-(l+3/2)} r^l e^{\frac{-r^2}{2b_s^2}} L_{n_r}^{l+1/2} \left( \frac{r^2}{b_s^2} \right) \left[ \frac{2l+1}{4\pi} \frac{(l-\Lambda)!}{(l+\Lambda)!} \right]^{1/2} P_l^{|\Lambda|*}(\theta) \frac{e^{-i\Lambda\phi}}{\sqrt{2\pi}} \right. \\ \left. \times \left[ \frac{2(n_\rho!)}{(n_\rho + |\Lambda|)!} \right]^{1/2} (b_d)^{-(\Lambda+1)} \rho^\Lambda e^{\frac{-\rho^2}{2b_d^2}} L_{n_\rho}^{|\Lambda|} \left( \frac{\rho^2}{b_d^2} \right) \frac{1}{(\sqrt{\pi} 2^{n_z} n_z!)^{1/2}} b_z^{-1/2} e^{\frac{-z^2}{2b_z^2}} H_{n_z} \left( \frac{z}{b_z} \right) \frac{e^{i\Lambda\phi}}{\sqrt{2\pi}} \right], \end{aligned} \quad (\text{B3})$$

where  $b_{s,d,z} = \sqrt{\frac{\hbar}{m\omega_{s,d,z}}}$  are oscillation parameters for spherical,  $\rho$ -radial, and  $z$  direction, respectively. The first and second factor are from the spherical HO, and the third and the fourth come from the deformed HO wave function.

The expansion of the deformed state  $|\alpha \Omega_\alpha \rangle \equiv |N n_z \Lambda_\alpha \Omega_\alpha \rangle$  into the spherical state  $|a \Omega_\alpha \rangle = |N_0 l \Lambda_\alpha \Sigma \rangle$  can be simply written as

$$|\alpha \Omega_\alpha \rangle = \sum_a B_a^\alpha |a \Omega_\alpha \rangle, \quad B_a^\alpha = \sum_{N n_z \Sigma} C_{l \Lambda_\alpha \frac{1}{2} \Sigma}^{j \Omega_\alpha} A_{N n_z \Lambda}^{N_0 l} b_{N n_z \Omega_\alpha}, \quad (\text{B4})$$

where  $B_a^\alpha$  is an expansion coefficient, and  $a$  and  $\alpha$  indicate quantum numbers of a nucleon state in a spherical and a deformed basis, respectively. Coefficients  $b_{N n_z \Omega_\alpha}$  are calculated from a deformed Woods-Saxon potential in the following way. In the cylindrical coordinate, eigenfunctions of a single particle state and its time-reversed state in a deformed Woods-Saxon potential are expressed as follows [29]:

$$\begin{aligned} |\alpha \rho_\alpha = +1\rangle = \sum_{N n_z} [b_{N n_z \Omega_\alpha}^{(+)} |N, n_z, \Lambda_\alpha, \Omega_\alpha = \Lambda_\alpha + 1/2\rangle + b_{N n_z \Omega_\alpha}^{(-)} |N, n_z, \Lambda_\alpha + 1, \Omega_\alpha = \Lambda_\alpha + 1 - 1/2\rangle], \\ |\alpha \rho_\alpha = -1\rangle = \sum_{N n_z} [b_{N n_z \Omega_\alpha}^{(+)} |N, n_z, -\Lambda_\alpha, \Omega_\alpha = -\Lambda_\alpha - 1/2\rangle - b_{N n_z \Omega_\alpha}^{(-)} |N, n_z, -\Lambda_\alpha - 1, \Omega_\alpha = -\Lambda_\alpha - 1 + 1/2\rangle], \end{aligned} \quad (\text{B5})$$

where the coefficients  $b_{Nn_z, \Omega_\alpha}^{(+)}$  and  $b_{Nn_z, \Omega_\alpha}^{(-)}$  are obtained from the eigenvalue equation of the total Hamiltonian in the deformed HO basis (Nilsson basis). The second terms in Eq. (B5) have the same projection  $\Omega_\alpha$  value as the first terms, but retain

another orbital angular momentum projection because of a flipped spin. Particle model space was exploited up to  $N = 5\hbar\omega$  for a deformed basis and up to  $N_0 = 10\hbar\omega$  for a spherical basis.

- 
- [1] H. T. Chen and A. Goswami, *Phys. Lett. B* **24**, 257 (1967).  
 [2] H. H. Wolter, A. Faessler, and P. U. Sauer, *Phys. Lett. B* **31**, 516 (1970).  
 [3] A. L. Goodman, *Phys. Rev. C* **58**, R3051 (1998).  
 [4] A. L. Goodman, G. L. Struble, J. Bar-Touv, and A. Goswami, *Phys. Rev. C* **2**, 380 (1970).  
 [5] A. L. Goodman, *Nucl. Phys. A* **186**, 475 (1972).  
 [6] F. Šimkovic, C. C. Moustakidis, L. Paceaescu, and A. Faessler, *Phys. Rev. C* **68**, 054319 (2003).  
 [7] J. Engel, S. Pittel, M. Stoitsov, P. Vogel, and J. Dukelsky, *Phys. Rev. C* **55**, 1781 (1997).  
 [8] O. Civitarese, M. Reboiro, and P. Vogel, *Phys. Rev. C* **56**, 1840 (1997).  
 [9] J. Engel, K. Langanke, and P. Vogel, *Phys. Lett. B* **389**, 211 (1996).  
 [10] W. Satula and R. Wyss, *Phys. Lett. B* **393**, 1 (1997).  
 [11] A. Gezerlis, G. F. Bertsch, and Y. L. Luo, *Phys. Rev. Lett.* **106**, 252502 (2011).  
 [12] Y. Y. Cheng, M. Bao, Y. M. Zhao, and A. Arima, *Phys. Rev. C* **91**, 024313 (2015).  
 [13] W. Satula, D. J. Dean, J. Gary, S. Mizutori, and W. Nazarewicz, *Phys. Lett. B* **407**, 103 (1997).  
 [14] W. Satula and R. Wyss, *Phys. Rev. Lett.* **86**, 4488 (2001); **87**, 052504 (2001).  
 [15] I. Bentley and S. Frauendorf, *Phys. Rev. C* **88**, 014322 (2013).  
 [16] K. Neergard, *Phys. Rev. C* **80**, 044313 (2009); **88**, 049901(E) (2013).  
 [17] K. Neergard, *Phys. Lett. B* **537**, 287 (2002); **572**, 159 (2003).  
 [18] N. Sandulescu, D. Negrea, J. Dukelsky, and C. W. Johnson, *Phys. Rev. C* **85**, 061303(R) (2012).  
 [19] D. Negrea and N. Sandulescu, *Phys. Rev. C* **90**, 024322 (2014).  
 [20] H. Matsubara *et al.*, *Phys. Rev. Lett.* **115**, 102501 (2015).  
 [21] E. Garrido, P. Sarriguren, E. Moya de Guerra, and P. Schuck, *Phys. Rev. C* **60**, 064312 (1999).  
 [22] E. Garrido, P. Sarriguren, E. Moya de Guerra, U. Lombardo, P. Schuck, and H. J. Schulze, *Phys. Rev. C* **63**, 037304 (2001).  
 [23] M. Sasano *et al.*, *Phys. Rev. Lett.* **107**, 202501 (2011).  
 [24] H. Sagawa, C. L. Bai, and G. Colo, *Phys. Scr.* **91**, 083011 (2016).  
 [25] S. Frauendorf and A. O. Miacchiavelli, *Prog. Part. and Nucl. Phys.* **78**, 24 (2014).  
 [26] H. Sagawa, T. Suzuki, and M. Sasano, *Phys. Rev. C* **94**, 041303(R) (2016).  
 [27] C. Qi and R. Wyss, *Phys. Scr.* **91**, 013009 (2016).  
 [28] B. Bulthuis and A. Gezerlis, *Phys. Rev. C* **93**, 014312 (2016).  
 [29] E. Ha and M.-K. Cheoun, *Nucl. Phys. A* **934**, 73 (2015).  
 [30] E. Ha and M.-K. Cheoun, *Phys. Rev. C* **88**, 017603 (2013).  
 [31] E. Ha and M.-K. Cheoun, *Phys. Rev. C* **94**, 054320 (2016).  
 [32] E. Ha, M.-K. Cheoun, and H. Sagawa, *Phys. Rev. C* **97**, 024320 (2018).  
 [33] E. Ha, M.-K. Cheoun, H. Sagawa, and W. Y. So, *Phys. Rev. C* **97**, 064322 (2018).  
 [34] G. Pantis, F. Šimkovic, J. D. Vergados, and Amand Faessler, *Phys. Rev. C* **53**, 695 (1996).  
 [35] M. K. Cheoun, A. Bobyk, A. Faessler, F. Šimkovic, and G. Teneva, *Nucl. Phys. A* **561**, 74 (1993); **564**, 329 (1993); M. K. Cheoun, A. Faessler, F. Šimkovic, G. Teneva, and A. Bobyk, *ibid.* **587**, 301 (1995).  
 [36] H. Jiang, G. J. Fu, Y. M. Zhao, and A. Arima, *Phys. Rev. C* **82**, 054317 (2010).  
 [37] Y. Urata, K. Hagino, and H. Sagawa, *Phys. Rev. C* **96**, 064311 (2017).  
 [38] P. Vogel and W. E. Ormand, *Phys. Rev. C* **47**, 623 (1993).  
 [39] P. Van Isacker, O. Juillet, and F. Nowacki, *Phys. Rev. Lett.* **82**, 2060 (1999).  
 [40] S. Raman, C. W. Nestor Jr., and P. Tikkanen, *At. Data and Nucl. Data Tables* **78**, 1 (2001).  
 [41] G. A. Lalazissis, S. Raman, and P. Ring, *At. Data and Nucl. Data Tables* **71**, 1 (1999).  
 [42] P. Moller, A. J. Sierk, T. Ichikawa, and H. Sagawa, *At. Data and Nucl. Data Tables* **109–110**, 1 (2016).  
 [43] H. Koura, T. Tachibana, M. Uno, and M. Yamada, *Prog. Theor. Phys.* **113**, 305 (2005).  
 [44] L. S. Kisslinger and R. A. Sorensen, *Rev. Mod. Phys.* **35**, 853 (1963).  
 [45] S. Cwiok *et al.*, *Comput. Phys. Commun.* **46**, 379 (1987).  
 [46] T. Oishi, K. Hagino, and H. Sagawa, *Phys. Rev. C* **90**, 034303 (2014); **82**, 024315 (2010); **82**, 069901(E) (2010).  
 [47] S. G. Nilsson and I. Ragnarsson, *Shapes and Shells in Nuclear Structure* (Cambridge University Press, Cambridge, 1995).